Hybrid Solar System for Decentralized Electric Power Generation and Storage

Nico Hotz
Department of Mechanical Engineering
and Materials Science,
Duke University,
303 Hudson Hall, P.O. Box 90300,
Durham, NC 27708-0300
e-mail: nico.hotz@duke.edu

The present study investigates the feasibility, efficiency, and system design of a hybrid solar system generating electric power for stationary applications such as residential buildings. The system is fed by methanol and combines methanol steam reforming and proton exchange membrane (PEM) fuel cells with solar collectors to generate the required heat for the steam reforming. The synergies of these technologies lead to a highly efficient system with significantly larger power densities compared to conventional systems and generate tremendous advantages in terms of installation and operation costs. The present investigation describes the entire proposed system and its components and presents first analytical, numerical, and experimental results of a larger project to prove the feasibility of such a system by analyzing first a bench test demonstrator generating around 10 W of electric power and finally a prototype for an entire single-family household. It is shown that the methanol-to-electricity efficiency of the entire system is above 50%.
[DOI: 10.1115/1.4007356]

Keywords: biomass, chemistry, collector, efficiency, energy, exergy, fluid flow, fuel, hydrogen, renewable, solar reactor, system, thermal power, thermodynamics

1 Introduction

Low-temperature fuel cells fed by hydrogen offer several advantages for generating electrical power, namely high energy and power densities per mass and volume, high energy conversion efficiencies, instantaneous recharging, and fast response to load changes. The most popular kind of fuel cells is the PEM fuel cell, which is already commercially available and can be operated with hydrogen feed at temperatures typically between 60 and 90 °C. However, due to the low energy density of hydrogen per volume, the storage of hydrogen within a relatively small fuel cell system in a building for long-term use is not only technically difficult, but as well very cumbersome and bulky. Therefore, a common solution in the literature is to store liquid hydrocarbon [1–7] or alcoholic fuels [8–14] and convert them to a hydrogen-rich reformate gas that can be subsequently used in a fuel cell. The use of methanol as primary fuel reduces the storage volume by up to 3 orders of magnitude, simplifies the recharging of the storage tank, and requires a much simpler distribution infrastructure than pressurized hydrogen.

Due to its reasonable energy density, very simple storage, easy availability, and especially due to the potential production from renewable sources, methanol is a highly appropriate fuel for a fuel cell system in combination with a steam reformer [15]. Methanol steam reforming on a Cu-based catalyst can be performed with a high efficiency resulting in a reformate gas containing up to 75% hydrogen. Since steam reforming of methanol is endothermic, the reactor has to be externally heated to reach and maintain the necessary reaction temperature. Such reformed methanol fuel cell (RMFC) systems are seen to have advantages compared to simpler direct methanol fuel cells (DMFC) due to their higher overall efficiency [15].

In recent years, the idea of analyzing a fuel cell-based energy conversion system by means of an exergy analysis has become popular [15–20]. In particular, when dealing with a solar-powered fuel cell system, an energetic analysis simply based on the first law of thermodynamics neglects a major point: A fair comparison and evaluation is needed for different qualities of energy, namely solar irradiance, chemical energy stored in fuels, heat, and finally, electrical energy. These different forms of energy provide different availabilities to be converted to useful work or, in other words, they comprise different exergy contents. A thorough exergetic analysis is the only way to adequately compare thermal, chemical, and electrical energy.

Most available literature deals with the exergetic analysis of innovative fuel cells, e.g., Refs. [15,18,20–25], conventional steam or gas turbine power plants [26–30], fuel cells combined with conventional power plants, e.g., Refs. [31–33], and solar photovoltaic devices, e.g., Refs. [34–37]. This exergetic analysis of single devices or simple systems is especially promising for cogeneration systems, where electrical power as well as thermal power can be used. Some researchers have been investigating the storage of thermal energy in the sense of exergy, e.g., Refs. [38–41]. Only few examples in the literature actually show innovative combinations of different types of energy conversion, such as fuel cells with solar heating [42].

A promising new idea is to combine the methanol steam reforming-fuel cell system with a solar thermal collector providing the required heat to the system in the form of sustainable and emission- and pollution-free solar energy. The main idea of this proposed project is to show how the efficiency of such a solar-powered fuel cell minipowerplant fed by methanol can be dramatically increased if solar energy is used as a heat source instead of other external heaters, e.g., fuel consuming burners. The goal of this study is to investigate a possibility to use sunlight as a major energy source to store chemical energy and generate electrical energy via solar thermal reformers in combination with fuel cells to improve efficiency and costs compared to conventional technologies.

In a recent numerical study [42], the hybrid solar system has been shown to achieve significant advantages both in terms of efficiency and cost for typical conditions found in Northern California (San Francisco Bay Area) when considering the conversion of sunlight and methanol to hydrogen and consequently the conversion of hydrogen to electricity in a fuel cell. However, the intermediate storage of hydrogen within the system has not been taken into account in the previous study [42]. The novelty of the present work is to integrate the storage of hydrogen in the system and to analyze

Contributed by the Solar Energy Division of ASME for publication in the JOURNAL OF SOLAR ENERGY ENGINEERING. Manuscript received December 11, 2011; final manuscript received July 20, 2012; published online September 21, 2012. Assoc. Editor: Wojciech Lipinski.

the effect of this gas storage component on the exergetic efficiency of the entire system.

2 Description of Entire System

The system analyzed in this study combines both technologies (low-temperature fuel cells and solar power) to achieve synergies in terms of cost and energetic efficiency compared to systems based on a single energy source and energy conversion technology. The entire system is shown in Fig. 1: First, the incoming mixture of liquid alcoholic fuel and water is evaporated and preheated to the reaction temperature by solar power. Typically, this reaction in the reformer takes place at temperatures between 200 and 250 °C, resulting in a reformer product gas containing up to 75% hydrogen. Since the reformate gas contains a small amount of carbon monoxide which is poisonous to the fuel cell, carbon monoxide is removed in the preferential oxidation (PROX) reactor following the reformer. The final gas mixture can be directly used in the proton exchange membrane (PEM) fuel cell or stored interim in a pressurized gas tank.

Direct solar-to-electric energy conversion, such as with photovoltaics, is currently not economically competitive with traditional electric power generation. Fuel cell technology directly using alcoholic fuel possibly generated from biomass (e.g., methanol) is not competitive in terms of costs either. The system proposed for this project consists of relatively cheap, commercially available hardware components (intermediate-temperature solar collector, pressurized gas tank, hydrogen-fed PEM fuel cell) and benefits in terms of energetic efficiency from the additional use of solar heat. The storage of liquid methanol as primary fuel in simple and safe tank requires an order of magnitude less space than a hydrogen gas tank (between 11 and 22 times less space for tank pressures of 150 and 75 bars, respectively, as shown later).

Additionally, the hybrid system with hydrogen as intermediate product benefits from the efficient short-term storage of a limited amount of hydrogen in a pressurized tank. When the energy consumption of a compressor for storing pressurized hydrogen is taken into account, the energetic efficiency of the gas storage amounts to about 94%, as shown later in this study. This allows for the temporary storage of energy in the system avoiding the need for expensive and inefficient electric energy storage, e.g., using batteries, reaching energetic efficiencies of around 65% for nickel-cadmium batteries and 75% for lead-acid batteries [43]. Only more expensive lithium-ion batteries can compete in terms of energetic efficiency with the proposed system, achieving 95% in average [43]. For electric power customers and electric grid companies, the on-site energy storage, e.g., in form of batteries or hydrogen and methanol tanks, leads to the significant advantage of a more controllable and highly flexible demand response since the stored hydrogen can be almost instantaneously converted to electric power by the fuel cell. This system configuration solves the problem of unbalanced power supply by sunlight during day and night, an intrinsic disadvantage of solar power. The proposed system can be operated without relying on power supply from the electric grid during peak hours in the early evening, as it is typical for residential buildings, when the power demand is high, but incoming solar power is already low.

Both solar collectors (e.g., for water heating applications) and low-temperature fuel cells exist as laboratory-scale bench test and as commercially available products. Nevertheless, to the best of the author's knowledge, there is no existing system or technology that uses solar power to heat an alcoholic biofuel reformer in combination with a hydrogen-fed fuel cell. The proposed novel hybrid system achieves significant advantages by finding a good compromise between installation cost, operation cost, and energetic efficiency compared to other technologies, e.g., photovoltaic energy conversion. Additionally, the intrinsic disadvantage of all purely solar systems, namely the limited power availability, is solved by the proposed system.

As previously described in more detail [44], the cost analysis of this proposed system shows a significant potential. If the system is designed to completely fulfill the power demand of a single-family household in summer, the combination of solar-heated methanol reforming, pressurized gas tank, and PEM fuel cell results in an estimated price per electric energy of 0.17 $/kWh (including the price for methanol fuel and the installation cost of approximately $6500, mainly the price for the fuel cell, solar collector, and catalysts). This is less expensive than a fossil fuel burning generator (0.52 $/kWh for natural gas) and much less than systems based on photovoltaic cells and Li-ion batteries (1.18 $/kWh electric energy), due to the high cost of photovoltaic cells and, particularly, batteries at their current state of development [43].

3 Description of System Components

3.1 Hybrid Reformer Integrated in Solar Collector. A crucial component of the proposed system is the solar-powered methanol steam reformer. Methanol steam reforming

$$CH_3OH + H_2O \rightarrow 3\,H_2 + CO_2 \quad (1)$$

is an endothermic reaction, requiring a heat input of 49.2 kJ per mole methanol. If the necessary enthalpy to vaporize water and methanol and to heat them to the typical reaction temperature of around 250 °C is included, 147.5 kJ of heat per mole methanol have to be provided to the reformer. In conventional systems, this heat is often generated by combusting part of the methanol input. However, this means that about 0.25 moles of methanol have to be burnt to generate enough heat to process 1 mole of methanol to hydrogen. If we include the intrinsic heat losses from the reformer to the ambient due to imperfect thermal insulation (for any reformer configuration, regardless of electric, chemical, or solar heating), even more methanol has to be allocated for heat generation in realistic applications. By using solar power to fulfill the heating requirement instead of combustion of precious fuel, the fuel-to-electricity efficiency is automatically increased by at least 25%, more realistically by at least 50% if heat losses of practical applications are included [42].

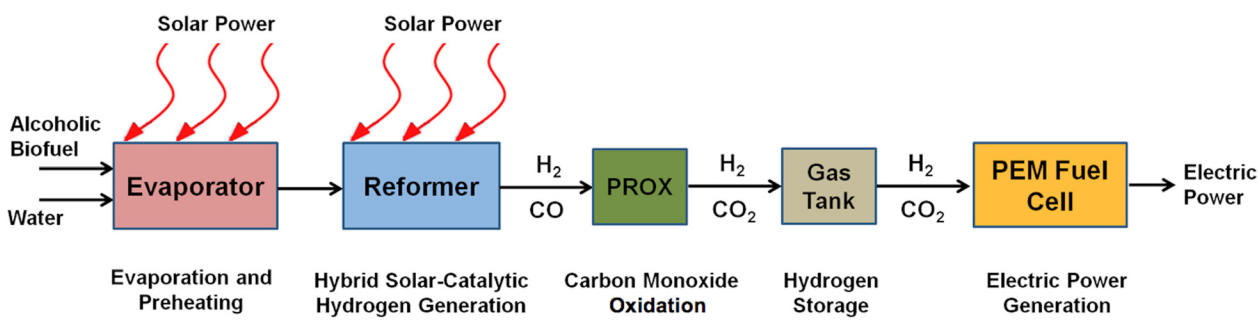

Fig. 1 Schematic of the hybrid solar-powered system

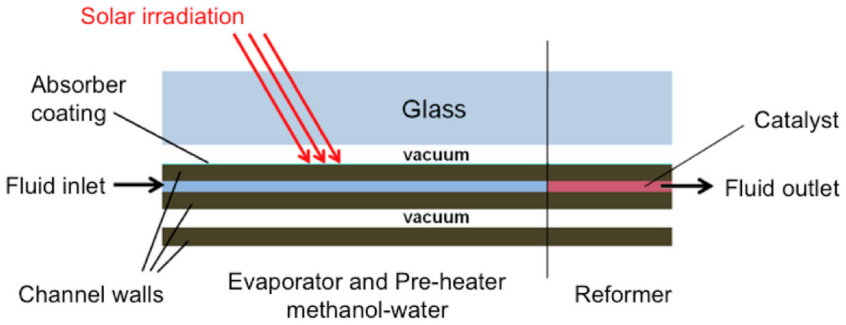

Fig. 2 Schematic of the hybrid reformer with integrated catalyst

The main issue of this system component is to design and fabricate a solar collector using available technology to reach a maximum temperature of 220–250 °C. This can be achieved by vacuum insulation around fluid channels and an efficient absorber coating around the fluid channel (Fig. 2).

The considered heat transfer mechanisms (convective heat transfer in the flow channels and on the external walls, radiative heat transfer, and conduction through all layers) are described in more detail in Ref. [42]. Due to the relatively high thermal conductivity of the solid layers, the temperature in the layers can be assumed to be constant and the fluid temperature across the flow direction is constant. The solar module is placed on top of the entire system and is therefore irradiated by sunlight, with the intermediate and PEM module underneath. The solar module is irradiated by sunlight at an angle of 90 deg.

It is assumed that the temperature in each glass layer and metallic channel wall is constant. There are no temperature gradients along the length, width, or height of each wafer. It has been shown that the conductive heat transfer in these layers is several orders of magnitude higher than all other heat transfer rates in the system. This is due to the high thermal conductivity of metal and even glass and it is confirmed by the Biot numbers for the glass layer and the metallic channel layers, being in the order of 10^{-2} and 10^{-3}, respectively. It can be said that the conductive heat transfer within the channel materials smoothes out any temperature variation immediately within these layers. Therefore, the temperature of all channel walls and glass layers has been assumed to be constant in the following calculations.

The temperature of the fluid flow varies markedly in the flow direction at the entrance of the modules and is almost constant after a short thermal entrance length. Temperature gradients in the fluid across the flow direction are neglected. The fluid temperature variation along the channels is slightly smoothed by conductive heat transfer in the fluid. Nevertheless, this conductive heat transfer is rather low compared to convective heat transfer (with thermal Peclet numbers significantly higher than unity) and especially when compared to the conductive heat transfer within the solid wafers, as described above, due to the low thermal conductivity of the fluids compared to the conductivity of the solid wafers (the thermal conductivities of glass and metal are more than 1 and 3 orders of magnitude larger than that of the mass flow, respectively).

The vapor–liquid equilibrium of a methanol–water binary mixture is calculated by using the Antoine equation to compute the saturation vapor pressure and the NRTL model to estimate the activity coefficients and consider nonideal mixing of the liquid phase by Renon and Prausnitz [45–47]. The best fitting model for the excess enthalpy of the liquid phase was found in Horstmann et al. [48]. The molar enthalpies for liquid and gas phase are calculated using polynomial expressions from Moran and Shapiro [49] and the DIPPR Project 801 database [50].

To quantitatively investigate the steam reforming of methanol, a reduced reaction model developed by Amphlett et al. [8] is applied, assuming that the reaction is dominated by the reforming reaction (1) and the decomposition of methanol, written as

$$CH_3OH \rightarrow 2\,H_2 + CO \tag{2}$$

Using a simple reactive flow model by Lee et al. [10], the reaction rate constants read

$$k_R = (A_R + B_R \cdot \ln\varphi_{\text{ref}}) \cdot \exp\left(-\frac{E_R}{R \cdot T_{\text{ref}}}\right) \cdot \rho_{\text{cat,ref}} \tag{3}$$

for the reforming reaction and

$$k_D = A_D \cdot \exp\left(-\frac{E_D}{R \cdot T_{\text{ref}}}\right) \cdot \rho_{\text{cat,ref}} \tag{4}$$

for the decomposition reaction. R is the universal gas constant and T_{ref} is the reformer temperature. The catalyst density in the packed bed $\rho_{\text{cat,ref}}$ and the kinetic parameters A_i, B_R, and E_i of the used $Cu/ZnO/Al_2O_3$ catalyst have previously been presented [15]. The reforming efficiency (or methanol conversion) is defined as

$$\eta_{\text{ref}} = \frac{\dot{n}_{CH_3OH,\text{in}} - \dot{n}_{CH_3OH,\text{out}}}{\dot{n}_{CH_3OH,\text{in}}} \tag{5}$$

It has been shown that temperatures of 240 or 250 °C can be achieved by solar irradiation without concentration of sunlight for reasonable flow rates [42,51]. By using a sophisticated vacuum insulation system and a highly efficient absorber material, stagnation temperatures above 400 °C can be reached.

3.2 Preferential CO Oxidation Reactor. Next to the desired methanol steam reforming reaction (1), unwanted thermal decomposition of methanol (2) will always take place, generating a small amount of CO, typically below 1% mole fraction. On the other hand, low-temperature PEM fuel cells are very sensitive to CO poisoning above 100 ppm. A straightforward solution to overcome this intrinsic problem of methanol reforming is the integration of a PROX reactor that oxidizes a large amount of the undesired CO in the reformate gas

$$CO + 0.5\,O_2 \rightarrow CO_2 \tag{6}$$

while reducing the precious H_2 only marginally. It has been shown that $Au/\alpha\text{-}Fe_2O_3$ catalysts are able to perform this task with high efficiency at 80 °C [42], typically containing approximately 3 wt. % Au. Applying the reaction rate constants measured by Kahlich et al. [52], the amount of reacted CO and H_2 can be calculated by

$$\frac{d\dot{n}_{CO}}{dV} = k_{CO} \cdot p_{O_2}^{\alpha_{O_2}} \cdot p_{CO}^{\alpha_{CO}} \cdot \rho_{\text{cat,PROX}} \tag{7}$$

and

$$\frac{d\dot{n}_{H_2}}{dV} = k_{H_2} \cdot p_{O_2}^{\alpha_{O_2}} \cdot \rho_{\text{cat,PROX}} \tag{8}$$

respectively, using data on the reaction kinetics from Kahlich et al. [52]. The molar inlet ratio between actual oxygen and stoichiometric oxygen is kept at a value of 2 ($\lambda_{PROX} = 2 \cdot \dot{n}_{CO_2,in}/\dot{n}_{O_2,in} = 2$).

3.3 Gas Storage Component. To complete the energy conversion system, an efficient storage component is required. A major advantage of the proposed stationary system is the simple, safe, and highly efficient storage of hydrogen as an intermediate product of the system. Using storage of the pressurized hydrogen-rich gas mixture in a tank can easily overcome the daily periods without sunshine, especially in the evening when the electric demand in a residential building is high, but little or no sunlight is available. Days of lower intensity of solar power can be compensated with stored hydrogen.

Based on the fuel cell model presented in an earlier study [42], the electric power consumption of a typical single-family household in central California during summer requires the conversion of approximately 21 m^3 hydrogen-rich gas mixture to electricity per day (at standard pressure and temperature). The maximum flow rate of product gas is around 3.57 m^3/h during peak period. To store the gas mixture, the usage of pressurized tanks is modeled. So-called type I gas tanks can store hydrogen at pressures up to 175 bars (made of aluminum) and up to 200 bars (made of steel). Type I tanks are relatively simple full-metal tanks and the first choice due to their limited costs. Types II–IV tanks are made of composites, containing aluminum or steel and fiberglass or carbon fiber. They can withstand pressures from 260 up to 660 bars; however, they are more sophisticated and therefore more expensive.

To store the hydrogen-rich gas mixture at pressures in the order of 75–150 bars, the gas has to be compressed in an oil-free, one- or multiple-stage compressor. Most commercial compressors are designed for higher flow rates; however, there are a considerable number of manufacturers offering small piston-metal diaphragm compressors for low hydrogen flow rates. As it can be seen from commercial examples [53–55], there are plenty of already available devices to compress low flow rates of hydrogen-rich gas mixture to high pressures up to 200 or even 450 bars. This calculation is based on an isentropic compression efficiency $\eta_{comp,s}$ of 80%, which is the efficiency guaranteed by most manufacturers of hydrogen compressors, leading to the following equation to calculate the compressor power P_{comp}:

$$P_{comp} = \frac{1}{\eta_{comp,s}} \cdot \dot{m}_{gas} \cdot c_p \cdot T_1 \cdot \left[\left(\frac{p_2}{p_1} \right)^{\frac{\kappa-1}{\kappa}} - 1 \right] \tag{9}$$

Additionally, a very promising solution for the future is the so-called guided rotor compressor (GRC). GRCs are positive displacement rotary gas compressors with the compression volume defined by a trochoidally rotating rotor mounted on an eccentric drive shaft. The typical compressor efficiency of GRCs has been determined as 80–85% [56]. GRCs are currently under research as hydrogen compressors for hydrogen stations. They are expected to achieve higher efficiencies than conventional piston-metal diaphragm compressors, excellent scalability, exceptional multistaging potential, lower noise levels, and high flexibility with regard to speed range, compression ratio, and inlet/outlet pressure. Due to these advantages, GRCs certainly have the potential to improve hydrogen compression in small systems once they are commercially prevalent.

3.4 PEM Fuel Cell. Finally, the low-temperature, hydrogen-fed PEM fuel cell has to be integrated into the entire system. PEM fuel cells are already commercially available and can be operated at temperatures typically between 60 and 90 °C with high efficiency.

The used fuel cell model is based on an analytical 1D model by Gurau et al. [57], assuming that the performance of a H_2-fed PEM fuel cell is determined by reaction and diffusion processes on the cathode side. The cell voltage E

$$E = E^0 - \Delta\Phi - \eta_s \tag{10}$$

is a function of the cathode surface overpotential η_s, the membrane phase potential between anode and cathode $\Delta\Phi$, and the ideal reversible voltage or Nernst potential E^0. The current density of the fuel cell i can be defined as a function of the surface overpotential η_s

$$i = n_e \cdot F \cdot k \cdot \exp\left(\eta_s \cdot \alpha_{ct} \cdot n_e \cdot \frac{F}{R \cdot T} \right) \cdot d_{cl} \cdot \Omega \cdot Y_{O_2} \tag{11}$$

where k is the reaction rate constant of the fuel cell reaction and d_{cl} is the thickness of the catalyst layer. The overall effectiveness factor Ω is given by Ref. [57]. By using the surface overpotential η_s as an independent parameter, the polarization curve can be described by Eqs. (10) and (11).

The 1D model of Gurau et al. [57] is extended to a quasi-2-D PEM fuel cell model, similar to Ref. [15]. The 1D model considers mass diffusion and reaction processes across the fuel cell. The temperature and species concentrations vary along the fuel cell and lead to a nonuniform current density distribution.

The anode-membrane-cathode assembly is assumed to be isothermal. The molar flow rates of H_2, water, and O_2 change along the fuel cell channels depending on the reaction rate, indicated by the current density i and an osmotic drag coefficient $n^d_{H_2O}$ for water transport through the membrane is calculated according to Ref. [58].

The combination of a hydrogen gas tank and a low-temperature PEM fuel cell lead to the tremendous advantage of a practically instantaneous demand response. Independent of solar availability and supply from the electric grid, the system can generate the required electric power whenever needed. This reduces the peak load for electric grid companies and power plant operators. On the other hand, the participation in dynamic demand response leads to cost savings for individual consumers, especially if the planned time-variant electric pricing will be implemented in the near future (meaning higher prices per electric energy unit during peak times).

The development of a PEM fuel cell optimized for the combination with an alcohol reformer is a crucial challenge. The optimization of the fuel cell has to take the specifications of a reformate gas as fuel input into account. In contrast to most studies, this fuel cell has to perform in an efficient manner if fed by a hydrogen-rich gas mixture (typically around 70–75% hydrogen) instead of pure or diluted hydrogen. The effect of byproducts in the reformate gas such as carbon dioxide and low amounts of carbon monoxide have to be considered. The fuel cell achieves a hydrogen conversion or utilization slightly above 80%, depending on the operating conditions. The cell with an active membrane area of 4.0 m^2 is operated at a cell voltage of 0.75 V and a temperature of 80 °C and achieves a maximum electric power output of 1607 W (indicating a moderate average power density of 40.3 mW/cm^2).

3.5 System Performance. The last and major part of this study is the integration of all four components (hybrid reformer, CO oxidation reactor, storage tank, and fuel cell) to a highly efficient, reliable, and cost-effective energy conversion and storage system.

An essential parameter of this study is the total exergetic efficiency μ_{tot} of the entire fuel cell power plant, defined as the ratio between the exergy output (i.e., the generated electric power P minus the required compressor power P_{comp}) and the exergy input (i.e., the exergy input of the solar radiation and the flow availability or exergy of methanol, water, and air at the inlets), given as

Table 1 Molar chemical availabilities $\bar{a}_{\text{chem},j}$ in kJ/mol

CH_3OH, liquid	718.0	H_2O, gaseous	9.5	N_2, gaseous	0.72
CH_3OH, gaseous	722.3	H_2, gaseous	236.1	CO_2, gaseous	19.87
H_2O, liquid	0.9	O_2, gaseous	3.97	CO, gaseous	275.1

$$\mu_{\text{tot}} = \frac{P - P_{\text{comp}}}{a_{\text{solar}} + a_{\text{CH}_3\text{OH,in}} + a_{\text{H}_2\text{O,in}} + a_{\text{air,in}}} \tag{12}$$

where the consumption of electrical power for the required pumping of the methanol–water mixture and the air flow through the system is neglected. The definition of the flow availabilities a_j is shown in Refs. [15,20], where the chemical availability $a_{\text{chem},\,j}$ is given by the reference environment model II of Table A-26 in Ref. [49]. The molar chemical availabilities for species relevant for this study are shown in Table 1.

To calculate the flow availability or exergy of a gas flow, the chemical availability is added to the thermodynamic exergy for each species j

$$\bar{a}_j = \left[\bar{h}_j(T) - \bar{h}_j(T_0)\right] - T_0 \cdot \left[\bar{s}_j(T) - \bar{s}_j(T_0)\right] + R \cdot T_0 \cdot \ln(X_j) + \bar{a}_{\text{chem},j} \tag{13}$$

where the molar enthalpies $\bar{h}_j$ and molar entropies $\bar{s}_j$ are calculated using polynomial expressions with parameters from Moran and Shapiro [49] and the DIPPR Project 801 database [50]. The solar exergy input can be calculated by

$$a_{\text{solar}} = I_{\text{solar,absorb}} \cdot \left(1 - \frac{T_0}{T_{\text{solar}}}\right) \tag{14}$$

according to Press [59] and Edgerton [60], where T_0 is the ambient temperature (=298 K) and T_{solar} is the black-body solar temperature (=5775 K). Since the solar radiation is a "cost-free" energy and exergy input, it is possible to define a chemical exergetic efficiency only considering the conversion of exergy in form of (chemical) flow availability to electric power:

$$\mu_{\text{chem}} = \frac{P - P_{\text{comp}}}{a_{\text{CH}_3\text{OH,in}} + a_{\text{H}_2\text{O,in}} + a_{\text{air,in}}} \tag{15}$$

Beside the exergetic efficiency, an important criterion is the power density per area, indicating how much electric power can be generated per area that is exposed to solar radiation. The resulting solar power density solar P''_{solar}

$$P''_{\text{solar}} = \frac{P}{A_{\text{solar}}} \tag{16}$$

can be used to compare the performance of the system with other area-based energy conversion techniques, especially with photovoltaic cells.

4 Results

As Hotz et al. [15] have shown by testing catalytic microparticles, for a realistic flow rate of methanol fuel, more than 230 °C are required to achieve between 85 and 90% of methanol conversion. For 240 °C, about 0.02 mg/s methanol input are possible using a reactor of 17.7 mm^3 volume and 15 mg catalyst. For 250 °C, a methanol mass flow rate of almost 0.04 mg/s can be achieved. Using these results to estimate the necessary size of the final steam reformer powering an entire single-family household, the following conclusions are drawn: The maximum methanol inlet mass flow rate is up to 0.28 g/s, requiring a reactor volume between 120 and 250 cm^3 and 105–210 g of catalyst, for reactor temperatures of 240–250 °C. It is believed that the required amount of catalyst can be reduced by applying nanoparticles instead of microparticles due to their larger surface-to-volume ratio.

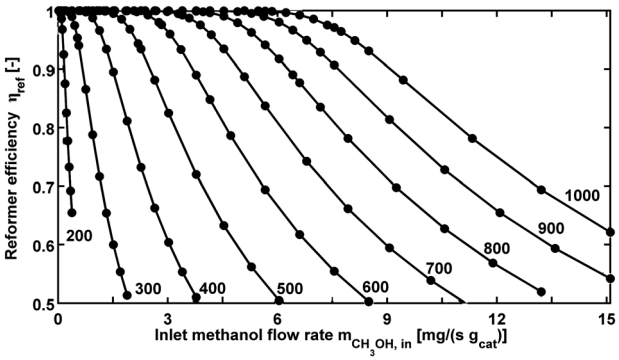

Fig. 3 Reformer efficiency depending on the solar irradiation (200–1000 W/m^2) for inlet flow rates varying from 0.19 to 15.1 mg/s methanol input per gram of catalyst

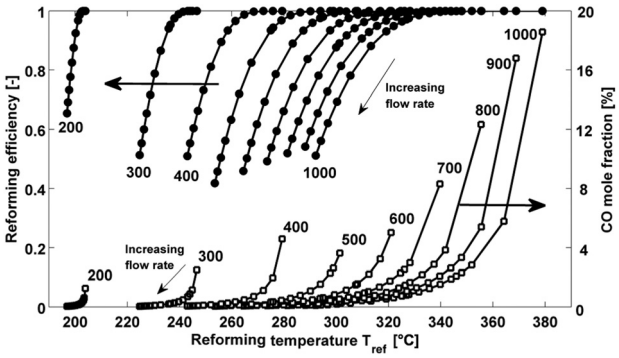

Fig. 4 Reforming efficiency, reformer temperature, and CO mole fraction of product gas depending on the solar irradiation (200–1000 W/m^2) for inlet flow rates varying from 0.19 to 15.1 mg/s methanol input per gram of catalyst

Figure 3 shows the reforming efficiency (or methanol conversion) as a function of methanol inlet mass flow per mass of catalyst and solar irradiation and Fig. 4 presents additionally the achieved reforming reaction temperature and the CO mole fraction of the product gas. It can be seen that for a maximum solar irradiation of 1000 W/m^2, 80% methanol conversion and a reforming temperature of 306.7 °C can be achieved at a methanol mass flow rate of 11.0 mg/(s g_{cat}), while generating a CO mole fraction of 0.28% in the reformate gas mixture. For 500 W/m^2 solar irradiation and 80% methanol conversion, a methanol flow rate of 3.2 mg/(s g_{cat}) results in a temperature of 266.3 °C and a CO mole fraction of 0.17%. In the PROX reactor, this amount of CO (below 0.3% CO mole fraction) can be successfully reacted, achieving CO mole fractions below 20 ppm for the fuel cell inlet gas at PROX reactor temperatures between 80 and 90 °C. For the following system analysis, the methanol inlet flow rate to the steam reformer is chosen to obtain a satisfactory compromise between high methanol conversion and low CO concentration.

For tests simulating a single-family household, relatively low storage pressures of 75, 100, 125, and 150 bars are compared, using simple type I tanks. These can be purchased for a few US$per liter of storage volume and have very long lifetimes. For the mentioned low storage pressures that are interesting for this system, this leads to a required tank volume between 1.0 m^3 (for 150 bars) and 2.0 m^3 (for 75 bars) to store the desired amount of hydrogen to power the single-family household for an entire week. Higher storage pressures are initially not desirable since they require more energy input for compression and more expensive tanks or vessels, despite the advantage of lower storage volumes.

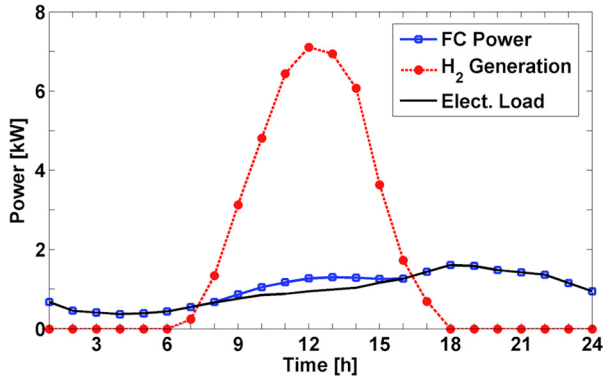

Fig. 5 Daily distribution of electric power load, electric output by the fuel cell, and generated hydrogen for a single-family household during an average day in summer in central California

In Fig. 5, the daily power generation and consumption for an average single-family household is shown for a typical day in summer in central California. From 6 p.m. to 6 a.m., no hydrogen is generated at all. At 7 a.m. and 5 p.m., some hydrogen is produced, but not enough to satisfy the electric load required for the household. Between 8 a.m. and 4 p.m., more hydrogen is generated than needed at these times and the excess hydrogen is stored for use in the evening, at night, and in the early morning. The peak production of hydrogen is equivalent to approximately 7 kWh at noon, corresponding to the maximum solar irradiation, with lower hydrogen generation due to less irradiation at other times. To generate enough hydrogen during the day, the system requires a solar collector area of 7.1 m^2 (5.2 m^2 for the evaporator and 1.9 m^2 for the reformer, shown in Fig. 6). The electric demand is directly satisfied by the fuel cell. Additionally, the fuel cell has to generate electric power to power the compressor during production of excess hydrogen from 8 a.m. to 4 p.m.

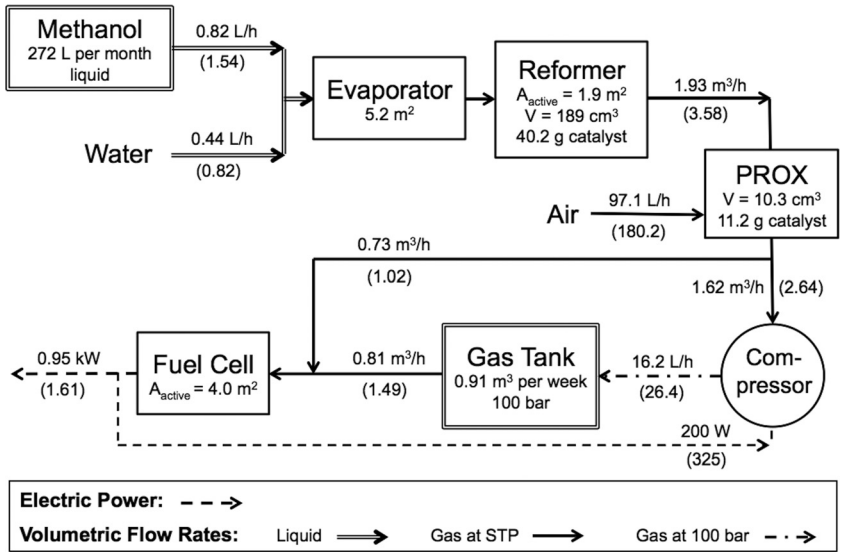

Fig. 6 Volumetric flow rates, electric power, and specifications of system components for single-family system in summer. Values for flow rates and electric power are shown as averages and (in parentheses) as maximum per hour. The averages are calculated for 11 h of sunshine (evaporator to PROX), 8 h of compressor operation, 16 h of discharging of the gas tank, and 24 h of fuel cell operation.

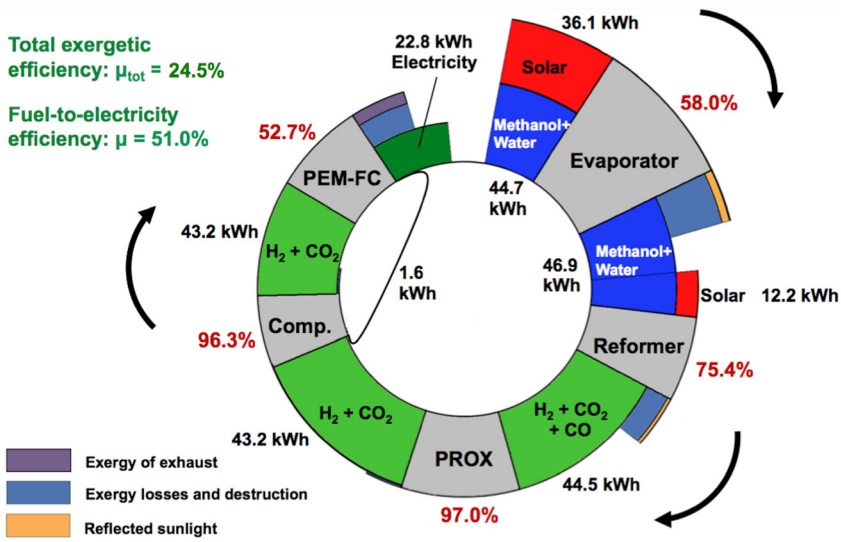

Fig. 7 Schematic of exergy flow through the entire system. Unless noted otherwise, all values show the exergy transfer during an entire day in summer (units: kWh).

In Fig. 6, the average liquid and gaseous volume flow rates through the system are shown (with maximum values in parentheses) for conditions in summer. A methanol fuel tank of 272 l contains sufficient methanol for 1 month of operation (based on conditions in summer). The evaporator of 5.2 m^2 solar collector area is fed with 0.82 l/h of methanol and 0.44 l/h of water in average between 7 a.m. and 6 p.m. and 1.54 l/h of methanol and 0.82 l/h of water at peak hour (between noon and 1 p.m.). The reformer consists of a solar collector area of 1.9 m^2, a reactor volume of 189 cm^3, and 40.2 g of $CuO/ZnO/Al_2O_3$ catalyst. The generated hydrogen-rich reformate gas amounts to 1.93 m^3/h in average and 3.58 m^3/h at noon. The PROX reactor is 10.3 cm^3 in volume and contains 11.2 g of Au/Fe_2O_3 catalyst. For the PROX reaction, the reformate gas is mixed in average with 97.1 l/h of air (180.2 l/h at peak hour). One part of the generated reformate gas is directly fed to the fuel cell, 0.73 m^3/h in average (between 7 a.m. and 6 p.m.) and a maximum 1.02 m^3/h (between 3 p.m. and 4 p.m.). The excess reformate gas (1.62 m^3/h in average and 2.64 m^3/h at maximum) is compressed to 100 bars and stored in a pressurized gas tank. The tank volume is 0.91 m^3 to store the entire reformate required for 1 week. Between 4 p.m. and 8 a.m., an average of 0.81 m^3/h of reformate gas is provided from the gas tank to the fuel cell. The fuel cell has an active membrane area of 4 m^2 and generates in average 0.95 kW of electric power for consumption and 200 W for the compressor during daytime (1.61 kW and 325 W, respectively, at peak).

In Fig. 7, the exergy flow for an entire summer day is presented. Almost equal amounts of chemical exergy in form of methanol and solar exergy are used as input (44.7 and 45.8 kWh, respectively). The steam reformer and PROX reactor convert this exergy to hydrogen with an efficiency of 46.5%, generating around 42 kWh in form of hydrogen. A bit more than a third of this hydrogen can be used directly in the fuel cell, generating 8.8 kWh of electric energy. The fuel cell itself has an exergetic efficiency of almost 58%, being determined by exergy destruction due to chemical reactions in the fuel cell, exergy losses due to heat losses, and incomplete conversion of hydrogen by the fuel cell (82% average hydrogen utilization). The majority of the hydrogen has to be temporarily stored, where the compression requires 1.6 kWh for a storage pressure of 100 bars. The indirect pathway generates finally 14 kWh of electric energy. The overall exergetic efficiency amounts to 25.2% (electric output divided by total exergy input). If the solar exergy input is neglected, the fuel-to-electricity efficiency is 51%. This overall efficiency is significantly higher than the efficiency of a fuel burning generator (for example, 14.5% for propane [44]) or a simpler DMFC system (25% [15]).

5 Conclusion

The present study analyzes possible opportunities, the efficiency, and a potential system design of a hybrid solar system generating electric power for stationary applications such as single-family households. The system is fed by methanol and combines methanol steam reforming and PEM fuel cells with solar collectors to generate the required heat for the steam reforming.

The results clearly show that a high efficiency can be achieved by using the combination of solar-powered steam reforming of methanol with PEM fuel cells. The fuel-to-electricity efficiency of the entire system is shown to be above 50%, even if the storage of hydrogen-rich gas in pressurized tanks is taken into account. The solar collector requires in summer a surface area of 7.1 m^2 exposed to sunlight and the PEM fuel cell membrane necessitates an area of 4.0 m^2. The storage tank for methanol to store sufficient fuel for 1 month of operation has to comprise of 272 l and the intermediate hydrogen storage tank contains 0.91 m^3 gas pressurized at 100 bars.

Nomenclature

a_i = (flow) availability of species i (W)
A, B = coefficient for reaction rate constants (mol kg^{-1} s^{-1})
A_{solar} = area irradiated by sunlight (m^2)
c_p = specific heat capacity (J kg^{-1})
d = height (across flow direction) (m)
E = cell voltage (V)
E^0 = Nernst potential (V)
$E_{R/D}$ = activation energy (J mol^{-1})
F = Faraday constant (=96,485 C mol^{-1})
$\bar{h}_i$ = enthalpy of species i (J mol^{-1})
i = current density (A m^{-2})
I_{solar} = intensity of solar radiation (W m^{-2})
k = reaction rate constants (mol m^{-3} s^{-1}) or (mol kg^{-1} s^{-1})
$\dot{m}_i$ = mass flow rate of species i (kg s^{-1})
$\dot{n}_i$ = molar flow rate of species i (mol s^{-1})
n_e = number of electrons
n^d = osmotic drag coefficient
p = pressure (Pa)
P = electrical power (W)
R = universal gas constant (=8.3145 J mol^{-1} K^{-1})
$\bar{s}_i$ = molar entropy of species i (J mol^{-1} K^{-1})
T = temperature (K)
V = volume (m^3)
X_i = mole fraction of gas phase i
Y_i = mass fraction of species i

Greek Letters

α_{ct} = charge transfer coefficient
$\alpha_{O2/CO}$ = coefficient for reaction rate constant
η_{ref} = reforming efficiency
$\eta_{comp,s}$ = isentropic compression efficiency
η_s = surface overpotential (V)
κ = heat capacity ratio
λ_{PROX} = excess molar O_2/CO ratio
μ_{chem} = chemical exergetic efficiency
μ_{tot} = total exergetic efficiency
ρ_{cat} = catalyst density (kg m^{-3})
φ_{ref} = molar water–methanol ratio at inlet
$\Delta\Phi$ = membrane phase potential (V)
Ω = overall effectiveness factor

Subscripts

0 = standard state (= 298 K, 101 kPa)
cl = catalyst layer
comp = compressor
D = decomposition reaction
PEM = PEM fuel cell
PROX = PROX reactor
R = reforming reaction
ref = steam reformer

Superscripts

" = per area (m^{-2})

References

[1] Aartun, I., Silberova, B., Venvik, H., Pfeifer, P., Gorke, O., Schubert, K., and Holmen, A., 2005, "Hydrogen Production From Propane in Rh-Impregnated Metallic Microchannel Reactors and Alumina Foams," Catal. Today, **105**(3–4), pp. 469–478.
[2] Bieberle-Huetter, A., Beckel, D., Infortuna, A., Muecke, U., Rupp, J., Gauckler, L., Rey-Mermet, S., Muralt, P., Bieri, N., Hotz, N., Stutz, M. J., Poulikakos, D., Heeb, P., Mueller, P., Bernard, A., Gmuer, R., and Hocker, T., 2008, "A Micro-Solid Oxide Fuel Cell System as Battery Replacement," J. Power Sources, **177**(1), pp. 123–130.
[3] Chaniotis, A., and Poulikakos, D., 2005, "Modeling and Optimization of Catalytic Partial Oxidation Methane Reforming for Fuel Cells," J. Power Sources, **142**(1–2), pp. 184–193.
[4] Hickman, D., and Schmidt, L., 1993, "Production of Syngas by Direct Catalytic-Oxidation of Methane," Science, **259**(5093), pp. 343–346.

[5] Hotz, N., Stutz, M. J., Loher, S., Stark, W., and Poulikakos, D., 2007, "Syngas Production From Butane Using a Flame-Made $Rh/Ce_{0.5}Zr_{0.5}O_2$ Catalyst," Appl. Catal., B, **73**(3–4), pp. 336–344.
[6] Laosiripojana, N., and Assabumrungrat, S., 2006, "Hydrogen Production From Steam and Autothermal Reforming of LPG Over High Surface Area Ceria," J. Power Sources, **158**(2), pp. 1348–1357.
[7] Silberova, B., Venvik, H., Walmsley, J., Holmen, A., 2005, "Small-Scale Hydrogen Production From Propane," Catal. Today, **100**(3–4), pp. 457–462.
[8] Amphlett, J. C., Creber, K. A. M., Davis, J. M., Mann, R. F., Peppley, B. A., and Stokes, D. M., 1994, "Hydrogen-Production by Steam Reforming of Methanol for Polymer Electrolyte Fuel-Cells," Int. J. Hydrogen Energy, **19**(2), pp. 131–137.
[9] Kundu, A., Jang, J., Lee, H., Kim, S., Gil, J., Jung, C., and Oh, Y., 2006, "MEMS-Based Micro-Fuel Processor for Application in a Cell Phone," J. Power Sources, **162**(1), pp. 572–578.
[10] Lee, M. T., Greif, R., Grigoropoulos, C. P., Park, H. G., and Hsu, F. K., 2007, "Transport in Packed-Bed and Wall-Coated Steam-Methanol Reformers," J. Power Sources, **166**(1), pp. 194–201.
[11] Lee, M. T., Hwang, D. J., Greif, R., and Grigoropoulos, C. P., 2009, "Nanocatalyst Fabrication and the Production of Hydrogen by Using Photon Energy," Int. J. Hydrogen Energy, **34**(4), pp. 1835–1843.
[12] Liguras, D., Goundani, K., and Verykios, X., 2004, "Production of Hydrogen for Fuel Cells by Catalytic Partial Oxidation of Ethanol Over Structured Ni Catalysts," J. Power Sources, **130**(1–2), pp. 30–37.
[13] Pattekar, A., and Kothare, M., 2005, "A Radial Microfluidic Fuel Processor," J. Power Sources, **147**(1–2), pp. 116–127.
[14] Suh, J. S., Lee, M. T., Greif, R., and Grigoropoulos, C. P., 2007, "A Study of Steam Methanol Reforming in a Microreactor," J. Power Sources, **173**(1), pp. 458–466.
[15] Hotz, N., Lee, M. T., Grigoropoulos, C. P., Senn, S. M., and Poulikakos, D., 2006, "Exergetic Analysis of Fuel Cell Micropowerplants Fed by Methanol," Int. J. Heat Mass Transfer, **49**(15–16), pp. 2397–2411.
[16] Yilanci, A., Dincer, I., and Ozturk, H. K., 2008, "Performance Analysis of a PEM Fuel Cell Unit in a Solar-Hydrogen System," Int. J. Hydrogen Energy, **33**(24), pp. 7538–7552.
[17] Granovskii, M., Dincer, I., and Rosen, M. A., 2008, "Exergy Analysis of a Gas Turbine Cycle With Steam Generation for Methane Conversion Within Solid Oxide Fuel Cells," J. Fuel Cell Sci. Technol., 5(3), p. 031005.
[18] Obara, S., and Tanno, I., 2008, "Exergy Analysis of a Regional-Distributed PEM Fuel Cell System," Int. J. Hydrogen Energy, **33**(9), pp. 2300–2310.
[19] Janardhanan, V. M., Heuveline, V., and Deutschmann, O., 2007, "Performance Analysis of a SOFC Under Direct Internal Reforming Conditions," J. Power Sources, **172**(1), pp. 296–307.
[20] Hotz, N., Senn, S. M., and Poulikakos, D., 2006, "Exergy Analysis of a Solid Oxide Fuel Cell Micropowerplant," J. Power Sources, **158**(1), pp. 333–347.
[21] Farhad, S., and Hamdullahpur, F., 2009, "Developing Fuel Map to Predict the Effect of Fuel Composition on the Maximum Efficiency of Solid Oxide Fuel Cells," J. Power Sources, **193**(2), pp. 632–638.
[22] Vargas, J. V. C., and Bejan, A., 2004, "Thermodynamic Optimization of Internal Structure in a Fuel Cell," Int. J. Energy Res., **28**(4), pp. 319–339.
[23] Mitchell, R. E., Gur, T. M., and Lee, A. C., 2009, "Thermodynamic Analysis of Gasification-Driven Direct Carbon Fuel Cells," J. Power Sources, **194**(2), pp. 774–785.
[24] Rashidi, R., Dincer, I., Naterer, G. F., and Berg, P., 2009, "Performance Evaluation of Direct Methanol Fuel Cells for Portable Applications," J. Power Sources, **187**(2), pp. 509–516.
[25] Toonssen, R., Woudstra, N., and Verkooijen, A. H. M., 2009, "Decentralized Generation of Electricity From Biomass With Proton Exchange Membrane Fuel Cell," J. Power Sources, **194**(1), pp. 456–466.
[26] Ameri, M., Ahmadi, P., and Hamidi, A., 2009, "Energy, Exergy and Exergoeconomic Analysis of a Steam Power Plant: A Case Study," Int. J. Energy Res., **33**(5), pp. 499–512.
[27] Dincer, I., Kanoglu, M., and Rosen, M. A., 2007, "Understanding Energy and Exergy Efficiencies for Improved Energy Management in Power Plants," Energy Policy, **35**(7), pp. 3967–3978.
[28] Gnanapragasam, N. V., Reddy, B. V., and Rosen, M. A., 2009, "Optimum Conditions for a Natural Gas Combined Cycle Power Generation System Based on Available Oxygen When Using Biomass as Supplementary Fuel," Energy, **34**(6), pp. 816–826.
[29] Kanoglu, M., and Dincer, I., 2009, "Performance Assessment of Cogeneration Plants," Energy Convers. Manage., **50**(1), pp. 76–81.
[30] Khaliq, A., and Choudhary, K., 2009, "Exergy Analysis of the Regenerative Gas Turbine Cycle Using Absorption Inlet Cooling and Evaporative Aftercooling," J. Energy Inst., **82**(3), pp. 159–167.
[31] Calise, F., Palombo, A., and Vanoli, L., 2006, "Design and Partial Load Exergy Analysis of Hybrid SOFC-GT Power Plant," J. Power Sources, **158**(1), pp. 225–244.
[32] Haseli, Y., Dincer, I., and Naterer, G. F., 2008, "Thermodynamic Modeling of a Gas Turbine Cycle Combined With a Solid Oxide Fuel Cell," Int. J. Hydrogen Energy, **33**(20), pp. 5811–5822.
[33] Rashidi, R., Berg, P., and Dincer, I., 2009, "Performance Investigation of a Combined MCFC System," Int. J. Hydrogen Energy, **34**(10), pp. 4395–4405.
[34] Joshi, A. S., Dincer, I., and Reddy, B. V., 2009, "Performance Analysis of Photovoltaic Systems: A Review," Renewable Sustainable Energy Rev., **13**(8), pp. 1884–1897.
[35] Joshi, A. S., Dincer, I., and Reddy, B. V., 2009, "Thermodynamic Assessment of Photovoltaic Systems," Sol. Energy, **83**(8), pp. 1139–1149.
[36] Kumar, S., and Tiwari, G. N., 2009, "Thermal Modelling, Validation and Exergetic Analysis of a Hybrid Photovoltaic/Thermal (PV/T) Active Solar Still," Int. J. Exergy, **6**(4), pp. 567–591.
[37] Tiwari, A., Sandhu, G. S., Barnwal, P., and Sodha, M. S., 2009, "Energy and Exergy Metrics Analyses of Hybrid Photovoltaic-Thermal Air Collector," Int. J. Exergy, **6**(5), pp. 729–748.
[38] Erek, A., and Dincer, I., 2009, "A New Approach to Energy and Exergy Analyses of Latent Heat Storage Unit," Heat Transfer Eng., **30**(6), pp. 506–515.
[39] Jack, M. W., and Wrobel, J., 2009, "Thermodynamic Optimization of a Stratified Thermal Storage Device," Appl. Therm. Eng., **29**(11–12), pp. 2344–2349.
[40] Kousksou, T., El Rhafiki, T., Arid, A., Schall, E., and Zeraouli, Y., 2008, "Power, Efficiency, and Irreversibility of Latent Energy Systems," J. Thermophys. Heat Transfer, **22**(2), pp. 234–239.
[41] Mawire, A., McPherson, M., and van den Heetkamp, R. R. J., 2009, "Thermal Performance of a Small Oil-In-Glass Tube Thermal Energy Storage System During Charging," Energy, **34**(7), pp. 838–849.
[42] Hotz, N., Zimmerman, R., Weinmueller, C., Lee, M.-T., Grigoropoulos, C. P., Rosengarten, G., and Poulikakos, D., 2010, "Exergetic Analysis and Optimization of a Solar-Powered Reformed Methanol Fuel Cell Micro-Powerplant," J. Power Sources, **195**(6), pp. 1676–1687.
[43] Electricity Storage Association, Technologies Database, 2009, http://www.electricitystorage.org/site/technologies/technology_comparisons
[44] Hotz, N., Pan, H., Grigoropoulos, C. P., and Ko, S. H., 2010, "Exergetic Analysis of Solar-Powered Hybrid Energy Conversion and Storage Scenarios for Stationary Applications," 4th International Conference on Energy Sustainability (ASME ES2010), Phoenix, AZ, May 17–22, ASME Paper No. ES2010-90255, pp. 879–888.
[45] Renon, H., Eckert, C. A., and Prausnitz, J. M., 1968, "Liquid-Liquid and Vapor-Liquid Equilibria for Binary and Ternary Systems With Dibutyl Ketone Dimethyl Sulfoxide N-Hexane and 1-Hexene," Ind. Eng. Chem. Process Des. Dev., **7**(2), pp. 220–225.
[46] Renon, H., Eckert, C. A., and Prausnitz, J. M., 1967, "Molecular Thermodynamics of Simple Liquids," Ind. Eng. Chem. Fundam., **6**(1), pp. 52–58.
[47] Renon, H., and Prausnitz, J. M., 1968, "Local Compositions in Thermodynamic Excess Functions for Liquid Mixtures," AIChE J., **14**(1), pp. 135–144.
[48] Horstmann, S., Mougin, P., Lecomte, F., Fischer, K., and Gmehling, J., 2002, "Phase Equilibrium and Excess Enthalpy Data for the System Methanol+2,2'-Diethanolamine Plus Water," J. Chem. Eng. Data, **47**(6), pp. 1496–1501.
[49] Moran, M. J., and Shapiro, D. N., 1999, *Fundamentals of Engineering Thermodynamics*, 4th ed., Wiley, New York.
[50] American Institute of Chemical Engineers/Design Institute for Physical Properties, 2009, DIPPR® Project 801—Evaluated Standard Thermophysical Property Values, Full Version.
[51] Zimmerman, R., Morrison, G., and Rosengarten, G., 2008, "A Solar Powered Microreactor for Hydrogen Production by Methanol Reforming," Proceedings of ASME 2nd International Conference on Energy Sustainability, Jacksonville, FL, ASME Paper No. ES2008-54202, pp. 391–396.
[52] Kahlich, M. J., Gasteiger, H. A., and Behm, R. J., 1999, "Kinetics of the Selective Low-Temperature Oxidation of CO in H_2-Rich Gas Over $Au/A\text{-}Fe_2O_3$," J. Catal., **182**, pp. 430–440.
[53] RIX Industries, Benicia, CA, http://www.rixindustries.com
[54] PDC Machines, Warminster, PA, http://www.pdcmachines.com
[55] Suction Gas Engine MFG, Tokyo, Japan, http://www.suction.co.jp
[56] Canadian Purcell Machinery, Eastport, ID, http://www.canadianpurcell.com
[57] Gurau, V., Barbir F., and Liu, H. T., 2000, "An Analytical Solution of a Half-Cell Model for PEM Fuel Cells," J. Electrochem. Soc., **147**(7), pp. 2468–2477.
[58] Springer, T. E., Zawodzinski, T. A., and Gottesfeld, S., 1991, "Polymer Electrolyte Fuel-Cell Model," J. Electrochem. Soc., **138**(8), pp. 2334–2342.
[59] Press, W. H., 1976, "Theoretical Maximum for Energy From Direct and Diffuse Sunlight," Nature, **264**, pp. 734–735.
[60] Edgerton, R. H., 1980, "Second Law and Radiation," Energy, **5**, pp. 693–707.